Journal of Chromatography A, 1227 (2012) 73–81

Contents lists available at SciVerse ScienceDirect

Journal of Chromatography A

journal homepage: www.elsevier.com/locate/chroma

Simulated moving bed starting conditions using an empirical model for S-shaped adsorption isotherms

Charles M. Grill[a,*], Stefanie Abel[b], Markus Juza[b,1], Elke Huthmann[b]

[a] Pfizer Inc., Eastern Point Road, Groton, CT 06340, USA
[b] Carbogen Amcis AG, Schachenallee 29, CH-5001 Aarau, Switzerland

ARTICLE INFO

Article history:
Received 23 June 2011
Received in revised form
30 November 2011
Accepted 13 December 2011
Available online 20 December 2011

Keywords:
S-shaped adsorption isotherms
Preparative chromatography
Simulated moving bed chromatography
Non-linear chromatography

ABSTRACT

Simulated moving bed (SMB) chromatography is a complicated process that generally requires modeling to determine starting conditions. Typically one uses the triangle theory to arrive at these starting conditions. The most common adsorption isotherm model used to construct the triangle is the Langmuir isotherm or an isotherm derived from the Langmuir isotherm. Often, modeling software supplied by the SMB manufacturer is used to determine the Langmuirian isotherm parameters. This proprietary approach, while successful in most cases, gives inaccurate results when the adsorption of one of the components is dominated by an S-shaped isotherm. Such failures require lengthy and expensive trial-and-error procedures to optimize the separation. In this paper, we apply an empirical model for S-shaped isotherms to the problem. With this isotherm model a triangle was constructed using the equilibrium dispersive model to simulate the SMB process. The starting conditions predicted by this approach were far more accurate than those determined by the proprietary approach.

1. Introduction

Simulated moving bed (SMB) chromatography has found success in the pharmaceutical industry, particularly in the separation of enantiomers [1,2]. Several important drugs use SMB in the manufacturing process [1]. However, most of the SMB separations are carried out at much smaller scales, for example in support of clinical trials. In such separations, where the campaign's duration is measured in days or weeks, the goal of modeling is to give reasonably accurate start up conditions so that only a few minor (and obvious) adjustments in flow rates and/or cycle time are needed to bring the separation into compliance with project specifications.

In recent years, the triangle theory has proven successful in determining SMB starting conditions [3]. The triangle theory is easily implemented when the adsorption of the separating species can be described in terms of the Langmuir isotherm or an isotherm derived therefrom. Simple algebraic expressions can then be used to construct the triangle plot [3,4]. For example, the modified Langmuir isotherm (Eq. (1)) is often used to model enantiomeric adsorption [3]:

$$q_i = \Gamma c_i + \frac{q_s b_i c_i}{1 + b_1 c_1 + b_2 c_2} \quad (1)$$

where the first term is a linear nonselective term with Γ as the proportionality constant, q_i is the concentration of enantiomer i in the stationary phase, q_s is the saturation concentration of the adsorbing enantiomers in the stationary phase, c_i is the concentration of enantiomer i in the mobile phase, and b_i is the adsorption/desorption equilibrium constant for enantiomer i.

In many pharmaceutical facilities, the Lico-HELP software supplied by the SMB manufacturer Novasep is used to determine the adjustable parameters (Γ, q_s, b_i) in Eq. (1). In our experience this approach is usually successful in giving reasonable SMB starting conditions, which implies that Eq. (1) can mimic many adsorption isotherms in the concentration ranges of interest. However, when the adsorption of one or more components is dominated by an S-shaped isotherm, the Lico-HELP approach has not been successful; thus, lengthy trial-and-error procedures, costly in both time and materials, have been required [1]. This is not surprising in that equation 1 lacks an inflection point which is characteristic of S-shaped isotherms [5]. In this paper an empirical adsorption isotherm is used to determine the SMB starting conditions for a chiral separation in which the adsorption of the later eluting enantiomer is dominated by an S-shaped isotherm.

* Corresponding author. Tel.: +1 860 686 1421; fax: +1 860 686 6329.
E-mail address: charles.m.grill@pfizer.com (C.M. Grill).
[1] Current address: DSM Nutritional Products AG, Hauptstrasse 4, CH-4334 Sisseln, Switzerland.

0021-9673/$ – see front matter © 2011 Elsevier B.V. All rights reserved.
doi:10.1016/j.chroma.2011.12.042

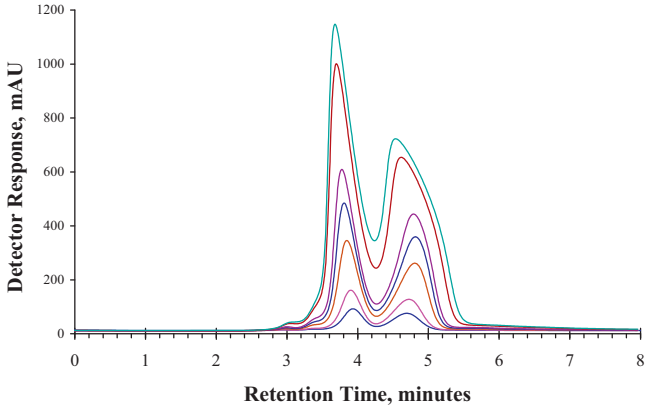

Fig. 1. Measured loading study of a pharmaceutical intermediate. Detector response (in milliabsorbance units, mAU) not corrected for nonlinearity. Stationary phase: Chiralpak AD 20 μm. Column dimensions: 0.46 cm × 25 cm. Mobile phase: ethanol/diethylamine, 100/0.1 (v/v). Feed concentration: 65 g racemate/L. Injection volumes: 10 μL, 20 μL, 50 μL, 75 μL, 100 μL, 200 μL, 250 μL.

2. Experimental

2.1. SMB separation (performed at Carbogen Amcis)

The compound whose separation is discussed in this paper is a proprietary chiral pharmaceutical intermediate synthesized at Pfizer Inc. The SMB separation of 6.31 kg of racemate was carried out at Carbogen Amcis (Aarau, Switzerland) using a Licosep Lab SMB system (Novasep, Pompey, France) equipped with eight Self-packer columns (Merck, Darmstadt, Germany) in a 2-2-2-2 configuration. Each column contained 110 g of Chiralpak AD (Daicel Chemical Industries, Ltd., Tokyo, Japan) and had bed dimensions of 4.8 cm (diameter) × 10 cm (length); the particle diameter was 20 μm. The mobile phase was ethanol/diethylamine, 100/0.1 (v/v). The feed solution was prepared by dissolving the racemate in mobile phase at a concentration of 66.1 g/L.

To determine the actual starting conditions, the Lico-HELP process development software (Revision 3) supplied by Novasep was used. A loading study similar in form to the one depicted in Fig. 1 was performed using a racemic solution (70 g/mL), and the retention time of the inflection point on each peak's leading edge was determined as a function of injection volume. Using these and other data listed in Table 1, the Lico-Help program determined the adjustable parameters in Eq. (1) through a proprietary fitting procedure. The values were: $\lambda = 0.80$, $q_s = 100$ g/L, $b_1 = 0.00020$ L/g, $b_2 = 0.0050$ L/g. Uncertainties are not reported as none were generated by the program. In accordance with the triangle theory, these parameters were then used to construct the right triangle shown in Fig. 2 [3].

Table 1
Loading study data used by Lico-HELP software to compute parameters for competitive isotherms defined in Eq. (1).

Injection volume (μL)	Estimated inflection point retention times (min)	
	Peak 1	Peak 2
10	3.92	4.63
20	3.90	4.67
50	3.85	4.75
75	3.81	4.75
100	3.78	4.73
200	3.71	4.58
250	3.69	4.51

Racemate concentration: 70 g/L.
Column dimensions: 0.46 cm × 25 cm.
Flow rate: 1.0 mL/min.
Bed bulk density: 0.60 g/mL.
Porosity, ε: 0.68.

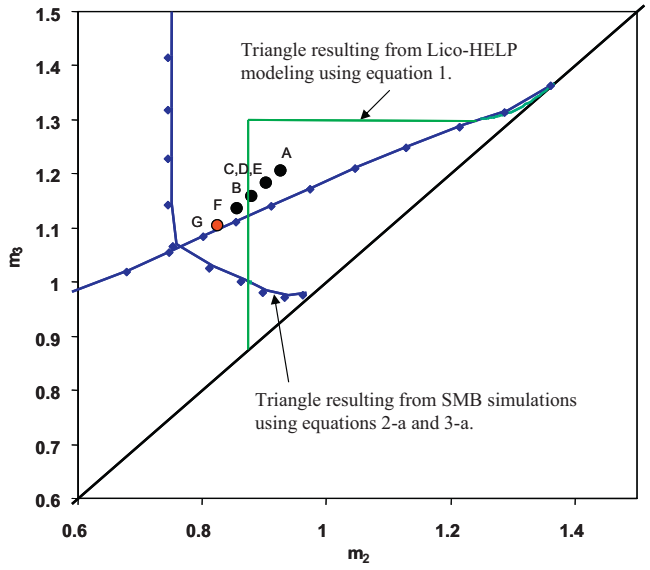

Fig. 2. Triangle plots for the SMB separation of the pharmaceutical intermediate, assuming a feed concentration of 70 g racemate/L. Right triangle, solid lines, no symbols: isotherm parameters determined by Lico-HELP software using Eq. (1) as the adsorption isotherm. Solid lines with symbols: Numerically constructed triangle (Section 3.2.2) using Eqs. (2a) and (3a) as the isotherms and the parameters listed in Table 4. Also depicted are the operating points for Conditions A–G shown in Table 3.

2.2. Loading study and adsorption isotherm determinations (performed at Pfizer Inc.)

2.2.1. Sample preparation

After the SMB separation was completed, the following nominal amounts of purified products were delivered to Pfizer from Carbogen for the purpose of adsorption isotherm determinations: 16.7 g of dry enantiomer 1 (raffinate) at 98.59% chiral purity (97.18% e.e.) and 13.5 g of dry enantiomer 2 (extract) at 99.37% chiral purity (98.74% e.e.). No achiral impurities were detected in either sample by analytical HPLC. These samples were judged to be of sufficient purity to determine the competitive adsorption isotherm parameters to two significant figure precision; thus, no further purification was performed.

Each sample was dried to constant weight (16.65 g and 13.38 g, respectively) using rotary evaporation at 60 °C. Initially two solutions of purified enantiomers were formed, each with a concentration of 130 g/L, by dissolving the dried samples in ethanol/diethylamine, 100/0.1 (v/v). In addition, two other solutions of purified enantiomers, each with a concentration of 6.5 g/L, were made by performing a 1/20 dilution of a portion of each original solution. Thus the following four solutions were prepared:

Solution 1: enantiomer 1 (from SMB raffinate), 130 g/L
Solution 2: enantiomer 2 (from SMB extract), 130 g/L
Solution 3: enantiomer 1, 6.5 g/L
Solution 4: enantiomer 2, 6.5 g/L

2.2.2. Apparatus

All loading studies and adsorption isotherm measurements were performed on an Agilent 1100 Series analytical chromatograph equipped with a diode array UV/visual detector (Agilent, Palo Alto, CA, USA). In all cases the mobile phase was ethanol/diethylamine 100/0.1 (v/v), the flow rate was 1.0 mL/min, and detection was at 275 nm. The column, whose dimensions were

Table 2
Perturbation method data: system peak retention times (t_{Ri}) versus concentration (c_i).

Enantiomer 1		Enantiomer 2	
c_1 (g/L)	t_{R1} (min)	c_2 (g/L)	t_{R2} (min)
0.65	3.97	0.65	4.70
1.3	3.94	1.3	4.74
2.0	3.94	2.0	4.81
2.6	3.91	2.6	4.83
3.3	3.86	3.3	4.81
6.5	3.77	6.5	4.79
13	3.58	13	4.33
26	3.34	26	3.79

0.46 cm (diameter) × 25 cm (length), was packed with Chiralpak AD, 20 μm particle size (Daicel Chemical Industries, Ltd., Tokyo, Japan).

2.2.3. Loading study

To produce the sample solution for the loading study, equal volumes of Solution 1 and Solution 2 were combined to give a racemic solution. A 1:1 dilution of this solution was then made with mobile phase to give a final racemic concentration of 65 g/L. The loading study consisted of injected volumes of 10 μL, 20 μL, 50 μL, 75 μL, 100 μL, 200 μL, and 250 μL of this solution.

Fig. 1 shows the loading study plots. The chromatograms were not corrected for detector nonlinearity as only a qualitative depiction of peak shapes was required. The retention times for enantiomer 1 decrease uniformly with loading. For enantiomer 2, the retention times increase with loadings through 75 μL; however, for loadings 100 μL through 250 μL, the retention times decrease. Thus, for loadings up to 75 μL, resolution actually increases with loading.

The existence of an S-shaped isotherm can often be discerned in a loading study. The retention time increases with loading in the early stages until the saturation concentration is approached, at which point retention times decrease with loading [6,7]. Peak 2 shows this behavior in our study. In Langmuirian adsorption, however, peak shapes generally skew to lower retention times with loading [4,8], as is the case with Peak 1.

2.2.4. Perturbation method measurements

To implement the perturbation method [9,10], the column was equilibrated with racemic solutions of various concentrations. These solutions were formed using the Agilent system's proportioning valve to mix equal amounts of two enantiomer solutions with the appropriate amount of mobile phase. The column was thermostated at 25 °C.

An analytical volume of mobile phase (50 μL) was injected at each step. As explained in Section 3.2.1, two system peaks eluted at retention times that depend non-trivially on the competitive adsorption isotherms [10]. The system peak retention times measured at various concentrations are shown in Table 2. Above a racemic concentration of 52 g/L, the system peaks merged, and accurate retention times could not be measured. An advantage of the perturbation method is that detector calibration is not required as only the determination of system peak retention times is performed [10].

The competitive isotherms cannot be determined directly with the perturbation method [9,10]. Rather, model isotherm equations were fit to the retention time data using an unweighted least squares process (Origin Scientific Graphing and Analysis Software, v. 7.5, OriginLab Corporation, Northampton, MA, USA).

3. Results and discussion

3.1. The SMB separation

The later eluting enantiomer was the desired component (enantiomer 2). However, the specifications of the SMB separation required ≥99.0% chiral purity (≥98.0% e.e.) for each enantiomer.

The right triangle shown in Fig. 2 was the result of the Lico-HELP modeling, and is indicative of linear competitive isotherms [3]. In Fig. 6a (dotted lines) the isotherms for enantiomers 1 and 2 are plotted along the diagonal of the c_1, c_2 plane, and indeed both isotherms are essentially linear. In the case of enantiomer 2, the initial increases in retention times with loading and the later decreases in retention times (see Fig. 1 and Table 1) were apparently interpreted by the modeling program as linear behavior.

The initial SMB flow rates, switch time, and purities (Conditions A) are shown in Table 3. As shown in Fig. 2, the operating point for these initial conditions is inside the right triangle determined by the Lico-HELP modeling procedure. Thus, the purity requirements should have been met for each enantiomer. As shown in Table 3, however, the purity specification was met for enantiomer 2 (extract) but not for enantiomer 1 (raffinate). Thus a multi-step trial-and-error procedure, costly in both time and materials, was required in order to bring both product streams into compliance with specifications. The conditions (Conditions A–G) and purity results for this multi-step procedure are also listed in Table 3. The operating point for each set of conditions is shown in Fig. 2.

3.2. Use of a two-site adsorption isotherm model to determine SMB conditions

In the loading study shown in Fig. 1, the retention time of the first peak (enantiomer 1) decreases with each loading. Such behavior is consistent with Langmuirian adsorption [4,8]. The retention time of the second peak initially increases with loading; at higher loadings the retention time reaches a maximum and begins to decrease. This suggests that the adsorption of enantiomer 2 is dominated by an S-shaped, Type V adsorption isotherm [6,7].

In this paper an empirical, thermodynamically consistent isotherm model is proposed to estimate SMB starting conditions when one or both components exhibit Type V adsorption behavior. This isotherm model postulates two types of adsorption sites: monomers of components 1 and 2 undergo competitive Langmuirian adsorption at site A, and homo-dimers of components 1 and 2 undergo Type V adsorption at site B. The Type V adsorption model is developed in Appendix A using straightforward statistical mechanical arguments.

The full model is expressed in the following equations

$$q_1 = q_{1A} + q_{1B} = \frac{q_{sA} b_{1A} c_1}{1 + b_{1A} c_1 + b_{2A} c_2} + \frac{q_{sB} b_{1B} c_1^2}{1 + b_{1B} c_1^2 + b_{2B} c_2^2} \quad (2)$$

$$q_2 = q_{2A} + q_{2B} = \frac{q_{sA} b_{2A} c_2}{1 + b_{1A} c_1 + b_{2A} c_2} + \frac{q_{sB} b_{2B} c_2^2}{1 + b_{1B} c_1^2 + b_{2B} c_2^2} \quad (3)$$

where q_i is the total concentration of species i in the stationary phase, q_{iA} is the concentration of species i in the stationary phase at site A (Langmuir adsorption of monomers), q_{iB} is the concentration of species i in the stationary phase at site B (Type V adsorption of homo-dimers), q_{sj} is the saturation concentration at site j, c_i is the concentration of species i in the mobile phase, and b_{ij} is the equilibrium constant for adsorption of species i at site j ($i = 1, 2$; j = A, B). All concentrations have units of g/L. There are six adjustable parameters: q_{sA}, q_{sB}, b_{1A}, b_{1B}, b_{2A}, and b_{2B}. One or more of the parameters can be set to zero.

Table 3
SMB conditions and results.

Run	Switch time (min)	Flow rates (mL/min)					Purity values (%)		Feed conc. (racemate) (g/L)
		Recycle	Eluent	Feed	Extract	Raffinate	Extract	Raffinate	
Conditions A	0.92	228.0	57.5	17.5	37.5	37.5	99.77	81.15	66.1
Conditions B	0.92	225.0	57.5	17.5	37.5	37.5	99.68	80.45	66.1
Conditions C	0.92	240.0	72.5	17.5	51.0	39.0	99.73	85.86	66.1
Conditions D	0.92	260.0	92.5	17.5	71.0	39.0	99.65	87.82	66.1
Conditions E	0.92	260.0	112.5	17.5	71.0	59.0	99.69	86.89	66.1
Conditions F	0.92	260.0	112.5	17.5	74.0	56.0	99.66	92.90	66.1
Conditions G	0.92	260.0	112.5	17.5	76.0	54.0	99.47	99.33	66.1

The isotherm model expressed in Eqs. (2) and (3) is empirical. The purpose of the model isotherm is to facilitate process development. No conclusions should be drawn about the actual adsorption mechanism. A similar model was suggested by Diack and Guiochon for the single component adsorption of phenyldodecane on porous carbon [7].

Theoretical loading study chromatograms were calculated using these model adsorption isotherm equations. To simplify the problem, an equilibrium dispersive model [11–13] was used instead of a complete model. With the equilibrium dispersive model a fixed plate number was used for each enantiomer (500 plates), and differences in mass transfer kinetics were not accounted for.

Depending on which, if any, of the parameters are set to zero, three types of loading study are predicted by the isotherm model. In the first case, none of the parameters is set to zero. Thus, competitive adsorption of monomers occurs at site A, and competitive adsorption of homo-dimers occurs at site B. An example is shown in Fig. 3a in which the adjustable parameters are: $q_{sA} = 86$ g/L, $b_{1A} = 0.0159$ L/g, $b_{2A} = 0.03193$ L/g, $q_{sB} = 19.77$ g/L, $b_{1B} = 0.00837$ L^2/g^2, $b_{2B} = 0.01$ L^2/g^2.

An example of the second case is shown in Fig. 3b in which b_{1B} is set to zero. The parameters are: $q_{sA} = 86$ g/L, $b_{1A} = 0.0103$ L/g, $b_{2A} = 0.03193$ L/g, $q_{sB} = 19.77$ g/L, $b_{1B} = 0.0$ L^2/g^2 (defined), $b_{2B} = 0.0084$ L^2/g^2. Eqs. (2) and (3) then become

$$q_1 = \frac{q_{sA} b_{1A} c_1}{1 + b_{1A} c_1 + b_{2A} c_2} \tag{2a}$$

$$q_2 = \frac{q_{sA} b_{2A} c_2}{1 + b_{1A} c_1 + b_{2A} c_2} + \frac{q_{sB} b_{2B} c_2^2}{1 + b_{2B} c_2^2} \tag{3a}$$

Because $b_{1B} = 0.00$, adsorbed dimers of enantiomer 1 do not form. Thus, competitive Langmuir adsorption of monomers occurs at site A, and single component adsorption of the dimers of enantiomer 2 occurs at site B.

In the third case, b_{2B} is set to zero. In Fig. 3c the parameters are: $q_{sA} = 86$ g/L, $b_{1A} = 0.0159$ L/g, $b_{2A} = 0.050$ L/g, $q_{sB} = 19.77$ g/L, $b_{1B} = 0.00837$ L^2/g^2, $b_{2B} = 0.0$ L^2/g^2 (defined). Eqs. (2) and (3) then become

$$q_1 = \frac{q_{sA} b_{1A} c_1}{1 + b_{1A} c_1 + b_{2A} c_2} + \frac{q_{sB} b_{1B} c_1^2}{1 + b_{1B} c_1^2} \tag{2b}$$

$$q_2 = \frac{q_{sA} b_{2A} c_2}{1 + b_{1A} c_1 + b_{2A} c_2} \tag{3b}$$

Because $b_{2B} = 0.00$, adsorbed dimers of enantiomer 2 do not form. Thus, competitive Langmuir adsorption of monomers occurs at site A, and single component adsorption of the dimers of enantiomer 1 occurs at site B.

To determine which variation of Eqs. (2) and (3) to use as the model isotherm, the experimentally measured loading study is compared to Fig. 3a–c. In our case, Fig. 1 is qualitatively similar to Fig. 3b. Thus, the adsorption of the pharmaceutical intermediate

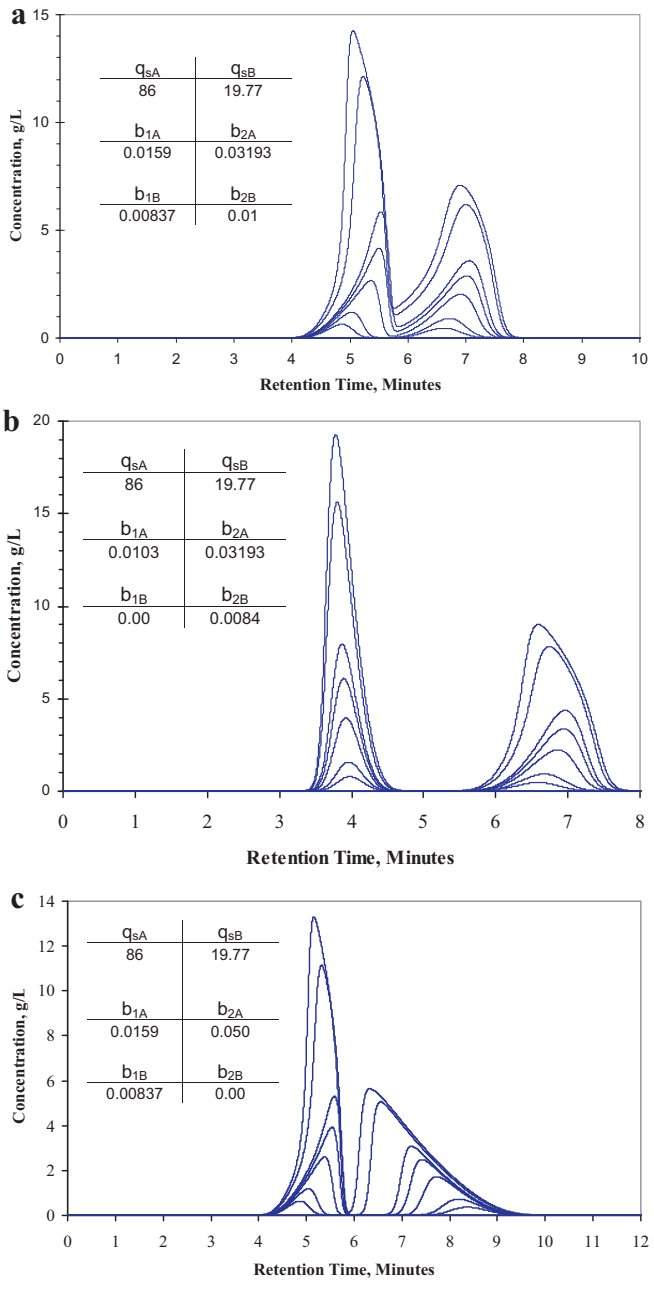

Fig. 3. (a) Modeled loading study. Parameter values: $q_{sA} = 86$ g/L, $b_{1A} = 0.0159$ L/g, $b_{2A} = 0.03193$ L/g, $q_{sB} = 19.77$ g/L, $b_{1B} = 0.00837$ L^2/g^2, $b_{2B} = 0.01$ L^2/g^2. See Eqs. (2) and (3). (b) Modeled loading study. Parameter values: $q_{sA} = 86$ g/L, $b_{1A} = 0.0103$ L/g, $b_{2A} = 0.03193$ L/g, $q_{sB} = 19.77$ g/L, $b_{1B} = 0.00$ L^2/g^2 (defined), $b_{2B} = 0.0084$ L^2/g^2. See Eqs. (2), (3) and (2a), (3a). (c) Modeled loading study. Parameter values: $q_{sA} = 86$ g/L, $b_{1A} = 0.0159$ L/g, $b_{2A} = 0.050$ L/g, $q_{sB} = 19.77$ g/L, $b_{1B} = 0.00837$ L^2/g^2, $b_{2B} = 0.00$ L^2/g^2 (defined). See Eqs. (2), (3) and (2b), (3b).

Table 4
Perturbation method results. Adsorption isotherm parameters determined by least squares fit of model Eqs. (2a) and (3a) to experimental data (Table 1 and Fig. 4). Errors are expressed in the 95% confidence interval. $R^2 = 0.99941$.

Site A			Site B	
q_{sA} (g/L)	b_{1A} (L/g)	b_{2A} (L/g)	q_{sB} (g/L)	b_{2B} (L^2/g^2)
86 ± 2	0.010 ± 0.001	0.016 ± 0.001	6.6 ± 0.3	0.0084 ± 0.0005

was modeled using Eqs. (2a) and (3a). The adjustable parameters were determined using the perturbation method.

3.2.1. Determination of competitive isotherm parameters using the perturbation method

The retention times of the system peaks, t_{R1} and t_{R2}, shown in Table 2 are related to the competitive adsorption isotherms through the following equations [10]:

$$t_{Rm}(c_1, c_2) = t_0 \left(1 + \frac{1-\varepsilon}{\varepsilon}\left(\frac{dq_1}{dc_1}\right)_{\text{Root } m}\right), \quad m = 1, 2 \tag{4a}$$

$$t_{Rn}(c_1, c_2) = t_0 \left(1 + \frac{1-\varepsilon}{\varepsilon}\left(\frac{dq_2}{dc_2}\right)_{\text{Root } n}\right), \quad n = 1, 2 \tag{4b}$$

where (dq_1/dc_1) and (dq_2/dc_2) are the total derivatives, and ε is the total bed void fraction of the column (in this study $\varepsilon = 0.676$). The total derivatives are derived from the roots of a quadratic equation (Eq. (7)); thus, Eqs. (4a) and (4b) appear to imply that there should be four retention times. However, the coherence condition requires that $(dq_1/dc_1) = (dq_2/dc_2)$; therefore, there can be only two unique system peak retention times [14]. These total derivatives are defined as:

$$\frac{dq_1}{dc_1} = \frac{\partial q_1}{\partial c_1} + \frac{\partial q_1}{\partial c_2}\frac{dc_2}{dc_1} \tag{5}$$

$$\frac{dq_2}{dc_2} = \frac{\partial q_2}{\partial c_2} + \frac{\partial q_2}{\partial c_1}\frac{dc_1}{dc_2} \tag{6}$$

Equating Eqs. (5) and (6) leads to the following equation, quadratic in (dc_1/dc_2):

$$\frac{\partial q_2}{\partial c_1}\left(\frac{dc_1}{dc_2}\right)^2 + \left(\frac{\partial q_2}{\partial c_2} - \frac{\partial q_1}{\partial c_1}\right)\left(\frac{dc_1}{dc_2}\right) - \frac{\partial q_1}{\partial c_2} = 0 \tag{7}$$

In calculating the system peak retention times using the isotherm equations, the following steps were followed:

a. The partial derivatives $(\partial q_2/\partial c_1, \partial q_2/\partial c_2, \partial q_1/\partial c_1, \partial q_1/\partial c_2)$ where calculated from Eqs. (2a) and (3a).
b. The derivatives (dc_1/dc_2) (roots 1 and 2) were calculated using Eq. (7).
c. The derivatives (dq_2/dc_2) (roots 1 and 2) were calculated using Eq. (6).
d. The system peak retention times, t_{R1} and t_{R2}, were calculated using Eq. (4b).

The least squares procedure described in Section 2.2.4 was used to find the values of the parameters in Eqs. (2a) and (3a) that led to the best fit to the measured system peak retention times. Plots of these results are shown in Fig. 4. The fit is excellent with an R^2 value of 0.99941. The optimized parameter values are listed in Table 4.

Fig. 5 shows plots of the isotherms for enantiomers 1 and 2 as determined by the perturbation method. The inflection in the isotherm for enantiomer 2 (q_2), which is indicative of an S-shaped isotherm [5], is difficult to discern. However, the partial derivatives are also plotted in Fig. 5. The maximum in $(\partial q_2/\partial c_2)$ indicates the existence of an inflection point in q_2. As expected, no indication of an inflection point is seen in the plot of q_1 or the plot of its partial derivative.

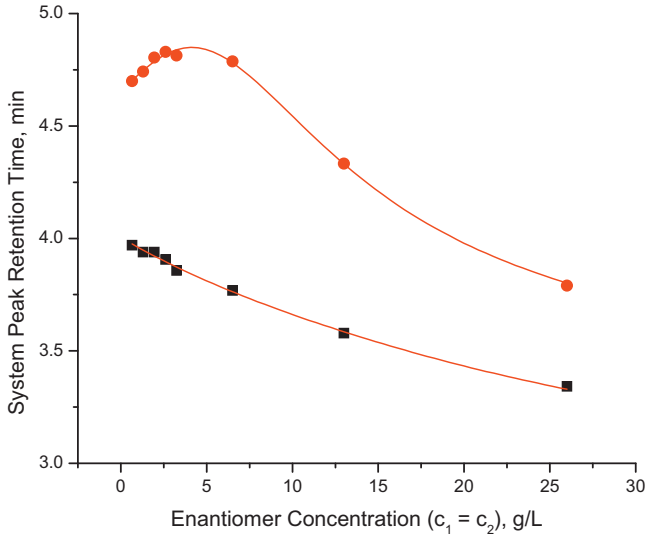

Fig. 4. Least squares fit of calculated to measured values of system peak retention times. These results were used to determine the adjustable parameters in Eqs. (2a) and (3a) using the perturbation method. Results of the fit are summarized in Table 4. Squares: measured t_{R1} values. Circles: measured t_{R2} values. Solid lines: calculated retention times.

3.2.2. Numerically produced triangle plot based on Eqs. (2a) and (3a)

Eqs. (2) and (3) had not been developed at the time the SMB separation was performed. To determine whether this model would have facilitated development of the SMB separation, a triangle plot was constructed numerically using Eqs. (2a) and (3a), and the parameters in Table 4. The triangle plot was constructed using a series of SMB simulations based on the equilibrium dispersive model [11–13]. An eight-column SMB system was simulated, and axial dispersion was accounted for by numerical dispersion (100 plates per column) [11]. The feed concentration was 70 g racemate/L.

It can be a daunting task to construct a triangle plot using SMB process simulations. One rather tedious way is to run a large number of simulations on grid points on the m_2–m_3 plane [2,23,24]. All operating points that result in pure extract and raffinate at steady state are within the region of complete separation. The accuracy of the resulting triangle borders depends on the chosen number of grid points in that area.

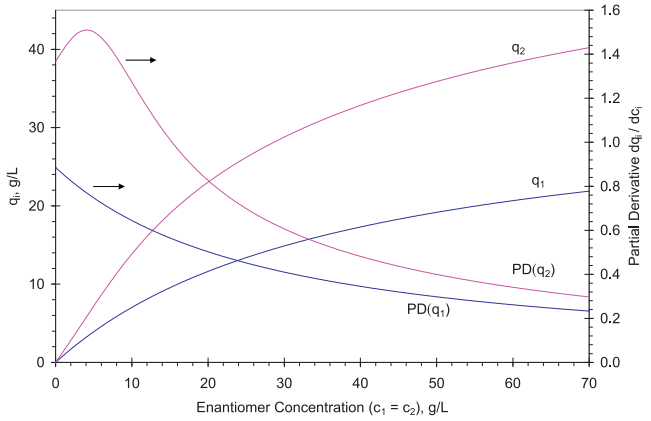

Fig. 5. Plots of competitive isotherms q_1 and q_2 along the diagonal of the c_1, c_2 plane ($c_1 = c_2$). Also plotted are the partial derivatives $(\partial q_1/\partial c_1)$ and $(\partial q_2/\partial c_2)$ ($PD(q_i) = \partial q_i/\partial c_i$). Eqs. (2a) and (3a) with the parameters listed in Table 4 were used in the calculations.

In our case a more efficient search algorithm was used to find the borders defining the four regions of the triangle plot. First, the Henry constants for Langmuir adsorption at site A ($H_i = q_{sA} b_{iA}$) were assumed to approximate the intersection points of the triangle sides with the diagonal; i.e., H_1, H_1 (0.86, 0.86) and H_2, H_2 (1.38, 1.38) were used to estimate these intersection points. These points were then chosen as the origins of vectors used to map the opposite sides of the triangle. The initial length of each vector was the distance between H_1, H_1 and H_2, H_2. Simulations were not run on the diagonal since the feed flow rate is zero along this line. Rather, each vector was rotated a small angle above the diagonal, and SMB simulations were then run at the tip of the vectors. For a given border across from point H_i, H_i, a steady state purity of component i between 99.89% and 99.90% (stop criterion) was regarded to be on the border. If the purity of component i was >99.90%, the length of the vector was increased; if the purity was <99.89%, the length was decreased. Simulations were run at each vector length until a border point was identified (the stop criterion was satisfied). To find the next border point, the vector's angle with the diagonal was increased by a small, defined amount. The initial length of a vector was the length of the previous vector used to find a border point. The process was repeated until all borders were identified.

It was not necessary to run every simulation until steady state was reached. As soon as it was clear that the target purity between 99.89% and 99.90% could not be reached, the simulation was stopped and the algorithm was allowed to make the next iteration at a new vector length. This made the procedure very efficient.

In this way two sets of simulations were performed. One set had the vector origin at H_1, H_1 and mapped the purity limits for the raffinate (component 1); this map defined the border between the triangle and the pure extract region (top border of the triangle), and the border between the pure raffinate region and the "no pure region". The other set, with vector origin H_2, H_2, mapped the pure extract borders (left border of the triangle, and the border between the pure extract region and the "no pure region"). Thus, the intersection of these two curves defined the four regions in the triangle plot: inside the triangle (both components pure), pure raffinate region, pure extract region, and the "no pure" region [3]. The resulting triangle plot is shown in Fig. 2.

Also shown in Fig. 2 are the operating points for Conditions A–G. The operating point for Conditions A is located well within the right triangle constructed using Lico-HELP modeling and Eq. (1). Thus, if this were the correct model, we would expect to see essentially pure extract and raffinate [3]. Similarly Conditions (B)–(E), being inside the right triangle, should have resulted in pure extract and pure raffinate. Finally, Conditions F and G should have resulted in pure raffinate. However, from the measured results listed in Table 3, all of these operating points, except for Conditions G, are within the pure extract region. The operating point for Conditions G appears to be within the pure extract and pure raffinate region, i.e. inside the true triangle. (For purposes of this discussion, we have defined a measured purity of ≥99% as "pure.")

These results are much more consistent with the triangle plot constructed numerically, where the operation points for Conditions (A)–(F) are clearly within the pure extract region [3]. The operating point for Conditions G, while in the pure extract region of the numerically constructed triangle plot, is very close to the triangle's boundary. Thus, initial operating conditions based on this triangle, in which the operating point would have been inside the numerically produced triangle, would have had an excellent chance of meeting the project specifications.

3.2.3. Triangle plot based on a Langmuirian fit to Eqs. (2a) and (3a)

In Fig. 6a, as previously mentioned, the isotherms calculated with the Lico-HELP program using Eq. (1) are plotted. Also plotted

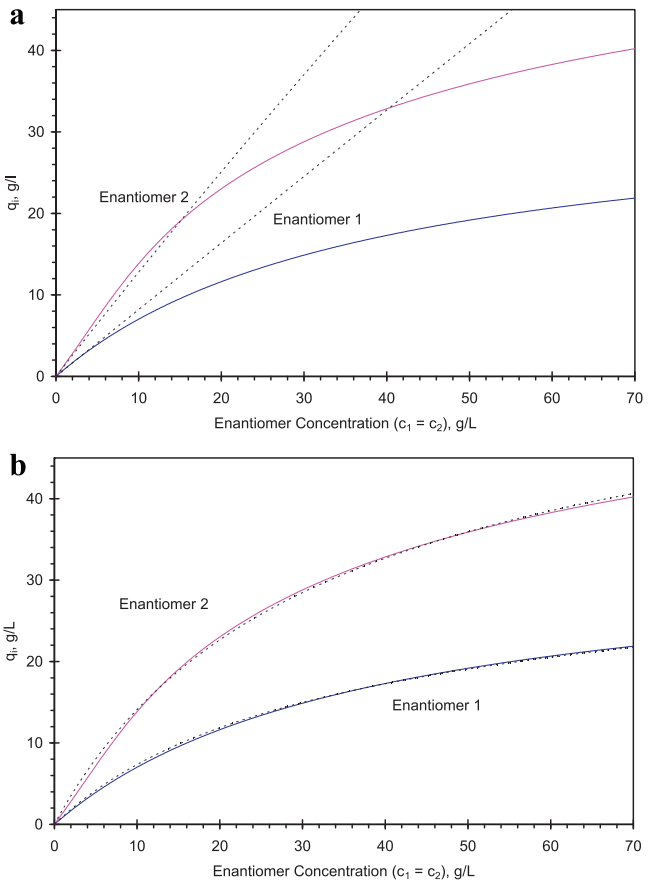

Fig. 6. (a) Solid curves: Diagonal plots ($c_1 = c_2$) of competitive adsorption isotherms calculated using Eqs. (2a) and (3a) with the parameters listed in Table 4. Dotted curves: Diagonal plots of modified Langmuir competitive adsorption isotherms (Eq. (1)) whose parameters were generated by the Lico-HELP program. (b) Solid curves: Diagonal plots ($c_1 = c_2$) of competitive adsorption isotherms calculated using Eqs. (2a) and (2b) with the parameters listed in Table 4. Dotted curves: Least squares fit of Eq. (1) to these calculated isotherms.

are the isotherms determined with the perturbation method using Eqs. (2a) and (3a). The agreement is poor except at very low concentrations.

As shown in Fig. 5, the inflection in the isotherm for enantiomer 2 (q_2) is slight. Thus it is surprising that the Lico-HELP program performed so poorly in fitting Eq. (1) to the data in Table 1.

An attempt was made (not shown) to fit Eq. (1) directly to the perturbation method retention times in Table 2. The fitted curve for enantiomer 2 did not exhibit a maximum and in general was a poor fit to the data. The curve for the enantiomer 1 data was also a poor fit. Thus this approach did not produce a viable triangle.

An approach that proved more successful was to force the curves generated by equation 1 to resemble as closely as possible the shape and magnitude of the isotherms calculated with Eqs. (2a) and (3a). A triangle plot was then easily constructed using the simple algebraic expressions described in reference [3]. To accomplish this, a least squares procedure was used to fit the adjustable parameters of Eq. (1) to the isotherms calculated by the perturbation method (Eqs. (2a) and (3a), and the optimized parameters in Table 4), all calculations occurring along the diagonal of the c_1, c_2 plane. The resulting optimized parameters for Eq. (1) were: $\lambda = 0.0290 \pm 0.0022$, $q_s = 83.3 \pm 0.6$ g/L, $b_1 = 0.0113 \pm 0.0001$ L/g, $b_2 = 0.0221 \pm 0.0002$ L/g. The fitted curves calculated with Eq. (1) (dotted curves) are shown in Fig. 6b. Also plotted are the isotherms calculated with Eqs. (2a) and (3a).

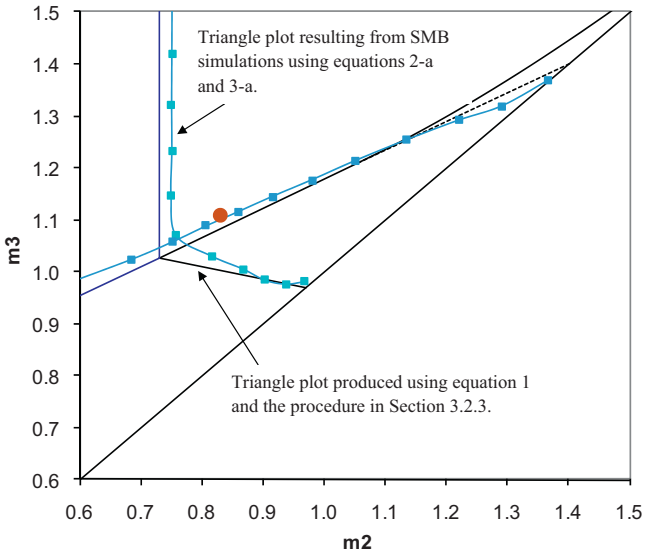

Fig. 7. Solid lines, no symbols: Triangle based on fit of Eq. (1) to the model isotherm Eqs. (2a) and (3a), and the parameters in Table 4 (See Section 3.2.3 and Fig. 6b). Solid lines, symbols: Also plotted for comparison is the numerically constructed triangle described in Section 3.2.2 and shown in Fig. 2. The large dot is the operating point for Conditions G in Table 3. Feed concentrations for both plots were 70 g racemate/L.

Except in the region of the inflection point in q_2, the fit is good ($R^2 = 0.99937$), and the errors in the parameters are reasonable.

The triangle plot generated from these fitted curves of equation 1 is shown in Fig. 7. For comparison, the triangle constructed numerically and the operating point for Conditions G are also plotted in Fig. 7. The two triangles are quite similar and would have produced similar initial SMB operating conditions.

In comparing Fig. 6a and b, it is evident that the approach described in this section was more successful than the Lico-HELP method in using Eq. (1) to approximate an S-shaped isotherm with slight inflection. It should be emphasized that in this procedure, we were not using Eq. (1) to model adsorption. Rather, we were using equation 1 as a function to approximate the adsorption isotherms expressed in Eq. (2a) and (3a). Using the optimized parameters for Eq. (1), the triangle plot was then quite easy to construct – a concern for those who do not have the means to construct the triangle plot numerically as described in Section 3.2.2.

4. Conclusions

The Lico-HELP procedure of determining SMB starting conditions in which adsorption is modeled using the modified Langmuir isotherm (Eq. (1)) has been shown to be inadequate when one component's adsorption is dominated by an S-shaped isotherm. This is consistent with earlier findings [1].

The procedure demonstrated in this paper, in which adsorption was modeled using Eqs. (2a) and (3a), produced much more accurate SMB starting conditions. The parameters of Eqs. (2) and (3) are easily obtained using the perturbation method: the experimental procedure is simple; detector calibration is not required for measurement of the loading study or system peak retention times; measurements are performed only on racemic mixtures at various concentrations (single component isotherms are not determined); determination of the adjustable parameters can be accomplished using commercially available software capable of fitting data to nonlinear functions.

Appling the triangle theory, however, is not straightforward. The more accurate procedure, calculating the triangle numerically using SMB simulations as described in Section 3.2.2, may not be available to everyone in industry. However, fitting the modified Langmuir isotherm (Eq. (1)) to the isotherms calculated with Eqs. (2) and (3) is quite simple. This method allows easy construction of the triangle plot, as discussed in Section 3.2.3. It is expected, therefore, that the procedure will be generally useful in developing process scale binary separations in which the adsorption of one or both components is characterized by an S-shaped isotherm.

Nomenclature

Subscripts

i	Component i ($i = 1, 2$)
j	Adsorption site j (j = A, B)
s	Designates saturation concentration in stationary phase

Latin symbols

a_i	Activity of species i
b_i	Adjustable parameter for species i, Eq. (1) [L/g]
b_{iA}	Adjustable parameter for species i at site A, Eqs. (2) and (3) [L/g]
b_{iB}	Adjustable parameter for species i at site B, Eqs. (2) and (3) [L^2/g^2]
c_i	Concentration of species i in liquid phase, Eqs. (1)–(3) [g/L]
k	Boltzmann's constant [J/K]
K_i	Equilibrium constant for species i, Eq. (A.22)
K_{ii}	Equilibrium constant for dimer i–i, Eq. (A.7)
M	Number of adsorption sites, Eq. (A.1)
m_i	Maximum number of species of type i adsorbed at the site, Eq. (A.2)
$\overline{N_i}$	Average number of molecules of species i adsorbed, Eq. (A.1)
q_i	Total concentration of species i in stationary phase, Eqs. (1)–(3) [g/L]
q_{ij}	Concentration of species i in stationary phase at site j, Eqs. (2) and (3) [g/L]; Eq. (A.8) [mole/L]
q_s	Saturation concentration of stationary phase, adjustable parameter, Eq. (1) [g/L]
q_{sj}	Saturation concentration at site j, adjustable parameter, Eqs. (2) and (3) [g/L]]; Eq. (A.8) [mole/L]
R	Gas constant [J/K/mole]
s_i	Number of molecules of species i adsorbed at the site, Eq. (A.2)
T	Temperature [K]
z	Site partition function, Eq. (A.3)

Greek symbols

Γ	Linear coefficient in modified Langmuir isotherm, Eq. (1)
ε	Total bed void fraction
$\in_j$	Adsorption energy of state j, Eq. (A.3) [J]
Θ_{ii}	Fractional occupation of adsorption sites by homo-dimer species ii, Eq. (A.7)
λ_i	Defined in Eq. (A.1)
λ_i°	Defined in Eq. (A.1)
μ_i	Chemical potential of species i, Eq. (A.9) [J/mole], Eq. (A.1) [J]
μ_j	Chemical potential of adsorption site B, Eq. (A.9) [J/mole]
μ_j°	Chemical potential of pure adsorption site j (no adsorbed component), Eq. (A.11) [J/mole]
Ξ	Grand partition function, Eq. (A.19)
ξ	Defined in Eq. (A.2)
Φ_j	Generalized pressure for site j, Eq. (A.11) [J/mole], Eq. (A.20) [J]

Appendix A.

A.1. Statistical mechanical derivation of the Type V adsorption model

In using statistical mechanics to construct a competitive adsorption isotherm model, the following relation is a convenient starting point [15]

$$\frac{\overline{N_i}}{M} = \lambda_i \left(\frac{\partial \ln \xi}{\partial \lambda_i} \right)_{T, \lambda_{j \neq i}} \tag{A.1}$$

where $\overline{N_i}$ is the average number of molecules of species i adsorbed, M is the number of adsorption sites, and

$$\lambda_i = e^{\mu_i/kT} = e^{(\mu_i^\circ/kT) + \ln a_i} = \lambda_i^\circ a_i$$

where a_i is the activity of component i, μ_i° is the chemical potential of i in the standard state, and $\lambda_i^\circ = e^{\mu_i^\circ/kT}$.

ξ having the form of a grand partition function, but for a single site, is defined as follows [15].

$$\xi = \sum_{s_1=0}^{s_1=m_1} \sum_{s_2=0}^{s_2=m_2} z(s_1, s_2) \lambda_1^{s_1} \lambda_2^{s_2} \tag{A.2}$$

where s_i is the number of molecules of species i adsorbed at the site; m_i is the maximum number of molecules of i that can be adsorbed at the site; and z is the partition function of the site, with s_1 molecules of species 1 and s_2 molecules of species 2 adsorbed at the site. The following expression defines z

$$z(s_1, s_2) = \sum_j e^{-\in_j(s_1, s_2)/kT} \tag{A.3}$$

where $\in_j$ is the energy of state j when s_1 molecules of 1 and s_2 molecules of 2 are adsorbed at the site, and the sum is over all possible energy states.

It is well known that quadratic functions can produce S-shaped isotherms [5]. Consider a two-component system in which a site can accommodate at most two adsorbed molecules, and in which adsorbate–adsorbate interactions occur between molecules adsorbed at the same site [15]. Let the potential energy of interaction between two molecules adsorbed on the same site be w_{ii} when two molecules of species i are adsorbed, or w_{12} when a molecule of 1 and a molecule of 2 are adsorbed. The possible site partition functions are then $z(0,0)$, $z(1,0)$, $z(0,1)$, $z(2,0)e^{-w_{11}/kT}$, $z(1,1)e^{-w_{12}/kT}$, and $z(0,2)e^{-w_{22}/kT}$. Eq. (A.2) then becomes

$$\xi = 1 + z(1,0)\lambda_1 + z(0,1)\lambda_2 + z(2,0)e^{-w_{11}/kT}\lambda_1^2 + z(0,2)e^{-w_{22}/kT}\lambda_2^2 + z(1,1)e^{-w_{12}/kT}\lambda_1\lambda_2 \tag{A.4}$$

Using Eq. (A.1) we obtain

$$\frac{\overline{N_1}}{M} = \frac{z(1,0)\lambda_1 + 2z(2,0)e^{-w_{11}/kT}\lambda_1^2 + z(1,1)e^{-w_{12}/kT}\lambda_1\lambda_2}{\xi} \tag{A.5.1}$$

$$\frac{\overline{N_2}}{M} = \frac{z(0,1)\lambda_2 + 2z(0,2)e^{-w_{22}/kT}\lambda_2^2 + z(1,1)e^{-w_{12}/kT}\lambda_1\lambda_2}{\xi} \tag{A.5.2}$$

Three assumptions will be made at this point in order to simplify the model. The goal is to construct an empirical model that that is thermodynamically consistent, that can be justified physically, that has the minimum number of adjustable parameters that will allow a good fit to the data, and that will yield accurate starting conditions for complex chromatographic processes such as SMB.

The first assumption is that w_{12} is large and positive, i.e. it is repulsive. This causes the last term in Eq. (A.4) to be negligible relative to the other terms. That is, it is assumed that the probability is negligible that an adsorbed hetero-dimer will form.

The second assumption is that the probability is very low that an adsorbed monomer of either species will form. Thus it is assumed that $z(1,0)\lambda_1 \ll 1$ and $z(0,1)\lambda_2 \ll 1$.The third assumption is that w_{11} and w_{22} are large and negative, i.e. they are attractive. This means that each adsorbed homo-dimer, 1–1 and 2–2, is much more likely to form than is the corresponding adsorbed monomer. For an adsorbed homo-dimer to form, however, two monomers in the gas phase or liquid phase must simultaneously be in the vicinity of the adsorption site. The probability of such an occurrence will be low at low pressures or concentrations, but will increase at moderate pressures or concentrations. Finally, the probability of adsorption will decrease at higher pressures or concentrations when the adsorption sites near saturation. Thus, an S-shaped isotherm will result.

With these assumptions, Eqs. (A.4) and (A.5) become

$$\xi = 1 + z(2,0)e^{-w_{11}/kT}\lambda_1^2 + z(0,2)e^{-w_{22}/kT}\lambda_2^2 \tag{A.6}$$

$$\frac{\overline{N_i}}{M} = \frac{2K_{ii}a_i^2}{1 + K_{11}a_1^2 + K_{22}a_2^2} = 2\Theta_{ii} \tag{A.7}$$

where $\overline{N_i}$ is the average number of (monomeric) molecules of species i adsorbed, M is the number of adsorption sites, Θ_{ii} is the fraction of sites occupied by i–i dimers, $K_{11} = z(2,0)e^{-w_{11}/kT}\lambda_1^{\circ 2}$ and $K_{22} = z(0,2)e^{-w_{22}/kT}\lambda_2^{\circ 2}$. In ideal systems, a_i, the activity of (monomeric) component i, can be replaced with either p_i (partial pressure) or c_i (concentration).

Macroscopically, we will be dealing with liquid chromatographic systems; thus, a_i will be replaced with c_i (liquid phase concentration of species i). Also, $\overline{N_i}$ will be replaced by q_{iB} (monomeric concentration of species i in the stationary phase, at site B). M will be replaced by q_{sB} (the concentration of adsorption sites B in the stationary phase; q_{sB} is also the saturation concentration of i–i dimers at site B; the saturation monomeric concentration of is $2q_{sB}$). Finally, K_{ii} will be replaced by b_{iB}. Eq. (A.7) then becomes

$$q_{iB} = \frac{2q_{sB}b_{iB}c_i^2}{1 + b_{1B}c_1^2 + b_{2B}c_2^2} \tag{A.8}$$

where all concentrations are in moles/L.

Eq. (A.8) is the simplest quadratic isotherm based on the competitive adsorption of dimers at individual sites. Thus, it requires the minimum number of adjustable parameters. If it were found that this model were not adequate in fitting the experimental data, a more complicated model could be constructed using Eqs. (A.4) and (A.5) for guidance.

A.2. Thermodynamic consistency

Empirical competitive adsorption isotherms are often used to aid development and optimization of chromatographic separations. The physical basis of such isotherms need not be an accurate reflection of the actual adsorption process [16]; however, it is common practice that the isotherms be thermodynamically consistent [17]. For any phase at equilibrium, this means that the Gibbs–Duhem equation (Eq. (A.9)) must be satisfied [22]. For an adsorbed phase involving two adsorbed components at constant temperature and pressure

$$-q_{sB}d\mu_B = q_{1B}d\mu_1 + q_{2B}d\mu_2 \tag{A.9}$$

where μ_B is the chemical potential of an adsorption site B, and μ_i is the chemical potential of adsorbed component i. The adsorbed phase consists of adsorption sites and the adsorbed species 1 and 2 [18].

At equilibrium, μ_i in the adsorbed phase is equal to μ_i in the liquid phase. Thus,

$$-\frac{q_{sB}}{RT}d\mu_B = q_{1B}(c_1, c_2)d\ \ln\ c_1 + q_{2B}(c_1, c_2)d\ \ln\ c_2 \tag{A.10}$$

where explicit notation has been made that in general q_{iB} is a function of the concentrations c_1 and c_2.

Integration of the left side of Eq. (A.10) is straightforward

$$-\frac{q_{sB}}{RT}\int_{\mu^{\circ}_{sB}}^{\mu_{sB}} d\mu_B = -\frac{q_{sB}}{RT}(\mu_B - \mu^{\circ}_B) = \frac{q_{sB}}{RT}\Phi_B \tag{A.11}$$

where μ°_B is the chemical potential of a pure adsorption site B (no adsorbed component), and $\Phi_B = -(\mu_B - \mu^{\circ}_B)$ [18,19]. Since μ°_B is a constant, $d\Phi_B = -d\mu_B$. Thus Eq. (A.9) can be rewritten as

$$q_{sB}d\Phi_B = q_{1B}d\mu_1 + q_{2B}d\mu_2 \tag{A.12}$$

Eq. (A.10) then becomes

$$\frac{q_{sB}}{RT}d\Phi_B = q_{1B}(c_1, c_2)d\ \ln\ c_1 + q_{2B}(c_1, c_2)d\ \ln\ c_2 \tag{A.13}$$

And Eq. (A.11) becomes

$$\frac{q_{sB}}{RT}\int_0^{\Phi} d\Phi_B = \frac{q_{Bs}}{RT}\Phi_B \tag{A.14}$$

Φ_B is a state function and can be thought of as a generalized pressure [15,18], having units of energy/mole. Thus the right side of Eq. (A.13) can be integrated along any convenient, physically justified route. As Φ_B is a state function, $d\Phi_B$ is an exact differential [20]. This property can be used as a convenient test for thermodynamic consistency.

Incorporating Eq. (A.8) into Eq. (A.13) we obtain

$$\frac{q_{sB}}{RT}\,d\Phi_B = \frac{2q_{sB}b_{1B}c_1}{1 + b_{1B}c_1^2 + b_{2B}c_2^2}\,dc_1 + \frac{2q_{sB}b_{2B}c_2}{1 + b_{1B}c_1^2 + b_{2B}c_2^2}\,dc_2 \tag{A.15}$$

where q_{sB} on the left side of Eq. (A.15) is the concentration of adsorption sites in the stationary phase.

Now,

$$\frac{\partial}{\partial c_2}\left(\frac{b_{1B}c_1}{1 + b_{1B}c_1^2 + b_{2B}c_2^2}\right) = \frac{\partial}{\partial c_1}\left(\frac{b_{2B}c_2}{1 + b_{1B}c_1^2 + b_{2B}c_2^2}\right) \tag{A.16}$$

The identity expressed by Eq. (A.16) is consistent with the status of Φ_B as a state function and $d\Phi_B$ as an exact differential. Thus Eq. (A.8) is thermodynamically consistent. It should be noted that this analysis, in which statistical mechanics is used to derive Eq. (A.7), explicitly requires that the saturation concentrations, expressed in molar units, to be equal for both species ($q_{sB1} = q_{sB2} = q_{sB}$).

Using similar arguments it can be shown that the first terms in Eqs. (2) and (3) (the competitive Langmuir isotherm) are thermodynamically consistent provided the saturation concentrations, expressed in molar units, are equal for both species ($q_{sA1} = q_{sA2} = q_{sA}$). This observation was first made by Kemball et al. [21]. Thus the first and second terms in Eqs. (2) and (3) are consistent with the Gibbs–Duhem equation (Eqs. (A.9) and (A.12)). By the general properties of differentiation, therefore, Eqs. (2) and (3) in their entirety are thermodynamically consistent.

A.3. Use of mass units

In Eqs. (2) and (3), all concentrations have units of g/L (these are the units most commonly used in industrial applications). This necessitates a minor change in Eq. (A.8), in which all concentrations are in molar units. At site B the saturation concentration of dimers in molar units is q_{sB}, and the saturation concentration of monomers is $2q_{sB}$. However, the mass of one mole of dimers is equal to the mass of two moles of monomers. Assuming the molecular weights of species 1 and 2 are equal, Eq. (A.8) becomes

$$q_{iB} = \frac{q_{sB}b_{iB}c_i^2}{1 + b_{1B}c_1^2 + b_{2B}c_2^2} \tag{A.17}$$

where all concentrations are expressed in units of g/L.

A.4. Explicit expressions for Φ_j

Φ_B (in units of energy/mole) can be derived by integrating Eq. (A.15) along any convenient path [e.g. ($c_1 = 0$, $c_2 = 0$) to ($c_1 = c_1$, $c_2 = 0$) to ($c_1 = c_1$, $c_2 = c_2$)]:

$$\Phi_B = RT\ \ln(1 + b_{1B}c_1^2 + b_{2B}c_2^2) \tag{A.18}$$

Using statistical mechanics, Φ_B (in units of energy/molecule) can also be determined as follows [15]:

$$e^{\Phi M/kT} = \Xi = \xi^M \tag{A.19}$$

$$\Phi = kT\ \ln\xi \tag{A.20}$$

where Ξ is the grand partition function. Using Eqs. (A.6) and (A.20) we find

$$\Phi_B = kT\ \ln(1 + K_{11}a_1^2 + K_{22}a_2^2) \tag{A.21}$$

Using similar arguments for Langmuir adsorption at site A, it can be shown that

$$\Phi_A = kT\ \ln(1 + K_1a_1 + K_2a_2). \tag{A.22}$$

References

[1] S. Abel, M. Juza, in: G. Subramanian (Ed.), Chiral Separation Techniques, third edition, Wiley-VCH Verlag GmbH & Co. KGaA, Weinheim, 2007, pp. 203–273.
[2] A. Rajendran, G. Paredes, M. Mazzotti, J. Chromatogr. A 1216 (2009) 709.
[3] M. Mazzotti, G. Storti, M. Morbedelli, J. Chromatogr. A 769 (1997) 3.
[4] M. Mazzotti, J. Chromatogr. A 1126 (2006) 311.
[5] G. Guiochon, A. Felinger, D.G. Shirazi, A.M. Katti, Fundamentals of Preparative and Nonlinear Chromatography, second edition, Academic Press, New York, NY, 2006, Chapter 3.
[6] A. Seidel-Morgenstern, G. Guiochon, Chem. Eng. Sci. 48 (1993) 2787.
[7] M. Diack, Guiochon, Anal. Chem. 63 (1991) 2608.
[8] G. Guiochon, S.G. Shirazi, A.M. Katti, Fundamentals of Preparative and Nonlinear Chromatography, Academic Press, Boston, MA, 1994, Chapter X.
[9] G. Guiochon, A. Felinger, D.G. Shirazi, A.M. Katti, Fundamentals of Preparative and Nonlinear Chromatography, Second edition, Academic Press, New York, NY, 2006, Chapter 4.
[10] C. Heuer, E. Küsters, T. Plattner, A. Seidel-Morgenstern, J. Chromatogr. A 827 (1998) 175.
[11] C. Migliorini, A. Gentilini, M. Mazzotti, M. Morbedelli, Ind. Eng. Chem. Res. 38 (1999) 2400.
[12] G. Guiochon, J. Chromatogr. A 965 (2002) 129.
[13] G. Guiochon, A. Felinger, D.G. Shirazi, A.M. Katti, Fundamentals of Preparative and Nonlinear Chromatography, second edition, Academic Press, New York, NY, 2006, Chapter 11.
[14] G. Guiochon, S.G. Shirazi, A.M. Katti, Fundamentals of Preparative and Nonlinear Chromatography, Academic Press, Boston, MA, 1994, Chapter VIII.
[15] T.L. Hill, An Introduction to Statistical Thermodynamics, Dover Publications, Inc., New York, NY, 1986, Chapter 7.
[16] K. Kaczmarski, D. Zhou, M. Gubernak, G. Guiochon, Biotechnol. Prog. 19 (2003) 455.
[17] E.I. Franses, F.A. Siddiqui, D.J. Ahn, C. Chang, L.N. Wang, Langmuir 11 (1995) 3183.
[18] D.M. Ruthven, Principles of Adsorption & Adsorption Processes, Wiley-Interscience, New York, NY, 1984, Chapter 3.
[19] T.L. Hill, J. Chem. Phys. 17 (1949) 520.
[20] E. Fermi, Thermodynamics, Dover Publications, Inc., New York, NY, 1936, Chapter 4.
[21] C. Kemball, E.K. Rideal, E.A. Guggenheim, Trans. Faraday Soc. 44 (1948) 948.
[22] F.C. Andrews, Thermodynamics: Principles and Applications, Wiley-Interscience, New York, NY, 1971, Chapter 13.
[23] K. Mihlbachler, A. Seidel-Morgenstern, G. Guiochon, AIChE J. 50 (2004) 611.
[24] M. Ballerstein, D. Michaels, A. Seidel-Morgenstern, R. Weismantel, Comput. Chem. Eng. 34 (2010) 447.